Cell Research (2009) 19:1150-1164.

www.nature.com/cr

ORIGINAL ARTICLE

Bystin-like protein is upregulated in hepatocellular carcinoma and required for nucleologenesis in cancer cell proliferation

Hanzhi Wang[1, 2], Wei Xiao[3], Qinbo Zhou[1, 2], Yun Chen[4], Shuo Yang[1], Jiansong Sheng[1], Yanqing Yin[2], Jia Fan[5], Jiawei Zhou[1, 2]

[1]Laboratory of Molecular Cell Biology, Institute of Biochemistry and Cell Biology; [2]State Key Laboratory of Neuroscience, Institute of Neuroscience, Shanghai Institutes for Biological Sciences, Chinese Academy of Sciences, Shanghai 200031, China; [3]Department of Pathology, First People's Hospital, Taizhou, Jiangsu 225300, China; [4]Department of Pathology, No. 411 Hospital, Shanghai 200081, China; [5]Key Laboratory for Carcinogenesis and Cancer Invasion, Liver Cancer Institute, Zhongshan Hospital, Shanghai Medical College of Fudan University, Shanghai 200032, China

The bystin-like (BYSL) gene was previously characterized to encode an accessory protein for cell adhesion that participates in early embryo implantation. It is also involved in 40S ribosomal subunit biogenesis and is found to be expressed in rapidly growing embryo and cancer cell lines. In order to explore the role of BYSL in cancer cell proliferation and growth, we used hepatocellular carcinoma (HCC) as a model. Here, we report that BYSL is crucial for HCC cell growth both *in vitro* and *in vivo*. Expression levels of BYSL mRNA and protein in human HCC specimens were markedly increased compared with those seen in adjacent non-cancerous tissue. *In vitro*, inhibition of BYSL by short hairpin RNA decreased HCC cell proliferation, induced apoptosis and partially arrested the cell cycle in the G2/M phase. *In vivo*, HCC cells treated with BYSL siRNA failed to form tumors in nude mice after subcutaneous implantation. To determine the cellular basis for BYSL RNAi-induced cell growth arrest, BYSL subcellular localization in mitotic and interphase HepG2 cells was examined. BYSL was present at multiple stages during nucleologenesis, including in nucleolus-derived foci (NDF), perichromosomal regions and the prenucleolar body (PNB) during mitosis. BYSL depletion remarkably suppressed NDF and PNB formation, and disrupted nucleoli assembly after mitosis, resulting in increased apoptosis and reduced tolerance of HCC cells to serum starvation. Taken together, our studies indicate that upregulated BYSL expression plays a role in hepatocarcinogenesis.

***Keywords*:** Bystin-like, nucleologenesis, nucleolar proteins, cell growth, hepatocellular carcinoma
Cell Research (2009) **19**:1150-1164. doi:10.1038/cr.2009.99; published online 18 August 2009

Introduction

Hepatocellular carcinoma (HCC) is one of the most prevalent malignancies worldwide with the highest prevalence in Southeast Asian countries and tropical Africa. In these regions, the incidence is estimated to be 10-20 per 100 000 population [1]. Like many malignancies, HCC has characteristics of fast cell proliferation and tumor growth, metastasis at an early stage, and poor response to treatment. Thus, further understanding of molecular mechanisms underlying HCC pathogenesis could improve our current efforts to screen for and treat this disease.

Accumulating evidence indicates that abnormalities in nuclear morphology and in the function of nucleolar proteins are closely associated with tumorigenesis. For example, pathologists use alterations in nucleolar

Correspondence: Jiawei Zhou
Tel/Fax: +86-21-5492-1073
E-mail: jwzhou@ion.ac.cn
Abbreviations: aa (amino acid); BYSL (bystin-like); FACS (fluorescence-activated cell sorter); GFP (green fluorescent protein); HCC (hepatocellular carcinoma); NDF (nucleolus-derived foci); NOR (nucleolar organizer regions); pAb (polyclonal antibody); PBS (phosphate-buffered saline); PNBs (prenucleolar bodies); PR (perichromosomal region); RNAi (RNA interference); rRNA (ribosomal RNA); Ubf (upstream binding factor)
Received 19 January 2009; revised 19 March 2009; accepted 13 April 2009; published online 18 August 2009

morphology as a diagnostic marker of malignancies. In particular, silver staining (AgNOR) has proven to be an important tool to predict clinical outcomes of some cancers [2]. Two major argyrophilic proteins responsible for such strong staining are B23 (also known as NPM1, nucleophosmin and nucleolar phosphoprotein B23) and nucleolin (also known as C23, NCL), both of which are nucleolar factors [3, 4] that participate in nucleolar reassembly at the end of mitosis [5]. Enhanced B23 expression causes uncontrolled cell growth, suggesting that it is not only a potential HCC marker but also may play a critical role in the progression of tumorigenesis [6]. Nucleolin has been described as both a marker and a protein functioning in tumorigenesis. Anti-cancer drugs targeting nucleolin have been described [7]. Recent evidence supports the idea that ribosomal proteins function in tumorigenesis. High levels of multiple large and small subunit ribosomal proteins have been found in several primary tumors, including HCC [8], leukemia and colon tumors [9-11]. Moreover, mutations in genes encoding DKC1 and the small ribosomal subunit protein S19, both of which directly affect ribosome assembly, are associated with increased cancer risk [12-14].

Bystin-like (BYSL) protein has recently also been identified as a nucleolar protein. It is involved in ribosomal processing of 18S rRNA, a component of the 40S subunit [15, 16], corroborating previous findings in yeast [17, 18]. It is also found that BYSL is highly expressed in human cervical cancer line HeLa cells, embryonic kidney 293T cells and embryonic stem cells [15, 16, 19]. Of interest, BYSL is a direct downstream target of the *c-myc* proto-oncogene, as evidenced in part by the fact that c-myc is shown to directly bind to the BYSL promoter in a B-cell line by CHIP assay [20]. *c-myc*, whose expression tightly correlates with the proliferative potential of the cell, is a key transforming agent in the etiology of human cancer [21, 22]. Amplification and overexpression of *c-myc* have been found in both chemical hepatocarcinogenesis in rat [23-25] and in human HCC cells [26-28]. Taken together, these data raise the possibility that BYSL may play important roles in rapid cell growth and proliferation seen in HCC.

In higher eukaryotes, the nucleolus is assembled during the end of mitosis. Proteins participating in pre-rRNA processing leave the nucleolus in prophase and some of them localize at perichromosomal regions (PR) during prometaphase and metaphase [29]. Some processing proteins transfer to nucleolus-derived foci (NDF) in the early anaphase cytoplasm [5]. During telophase, NDF disappear with a concomitant appearance of concentrated foci called prenucleolar bodies (PNBs) in the reforming nuclei [30-33]. Although it is not clear why intermediate steps including NDF and PNBs are required, formation of NDF and PNBs is crucial for nucleolar assembly.

In the present study, we tested the hypothesis that the ribosomal protein BYSL contributes to tumorigenesis through altered nucleologenesis. We demonstrate that BYSL expression levels are markedly upregulated in human HCC specimens. Suppression of BYSL expression resulted in impaired nucleologenesis, leading to retarded cell growth and failure of tumor formation in nude mice. Our data suggest that BYSL is critical for HCC growth and nucleologenesis.

Results

Upregulated BYSL expression in HCC

To characterize BYSL expression in HCC, we first determined the specificity of a polyclonal antibody (pAb) raised in our laboratory against human BYSL. As shown in Figure 1, BYSL antibody recognized exogenous and endogenous BYSL in HepG2 cells transfected with pEGFP-BYSL in western blotting assays. Exogenous GFP-BYSL fusion protein (~76 kDa) was also recognized by a GFP antibody (Figure 1A). Immunofluorescence showed that the BYSL antibody recognized only endogenous nucleolar signals, consistent with the pattern of exogenous GFP-BYSL fluorescence (Supplementary information, Figure S1A). Immunostaining using pre-immune serum showed no positive signal (Supplementary information, Figure S1B). These data suggest high antibody specificity and selectivity, agreeing with reports that BYSL (*Enp1*) is found in the nucleolus of yeast, trophoblasts and cancer cell lines [15-18].

Using this antibody, 98 paraffin-embedded human HCC specimens and adjacent non-cancerous liver tissues were subjected to immunohistochemical analysis. Figure 1B shows morphology of HCC cells indicating higher BYSL expression than that seen in adjacent liver tissue. In HCC tissue, liver cell structure was severely distorted with prominent BYSL staining in both HCC cells and vascular endothelial cells (Figure 1B, panel b to d). Strong BYSL immunoreactivity was observed in both the cytosol and nucleus of HCC cells. In some cases, nuclear localization of BYSL immunosignals was stronger than that in the cytoplasm (Figure 1B, panel b). In contrast, in normal liver tissue most liver cells either lacked BYSL immunoreactivity or showed light nuclear and cytoplasmic staining (Figure 1B, panel a). Pseudoglandular structures, which often appear in HCC [34] were seen in HCC specimens and showed strong BYSL immunoreactivity (Figure 1B, panel c). This pattern resembled that of glandular epithelia cells in mouse uteri after implantation [19]. Furthermore, as shown in Figure

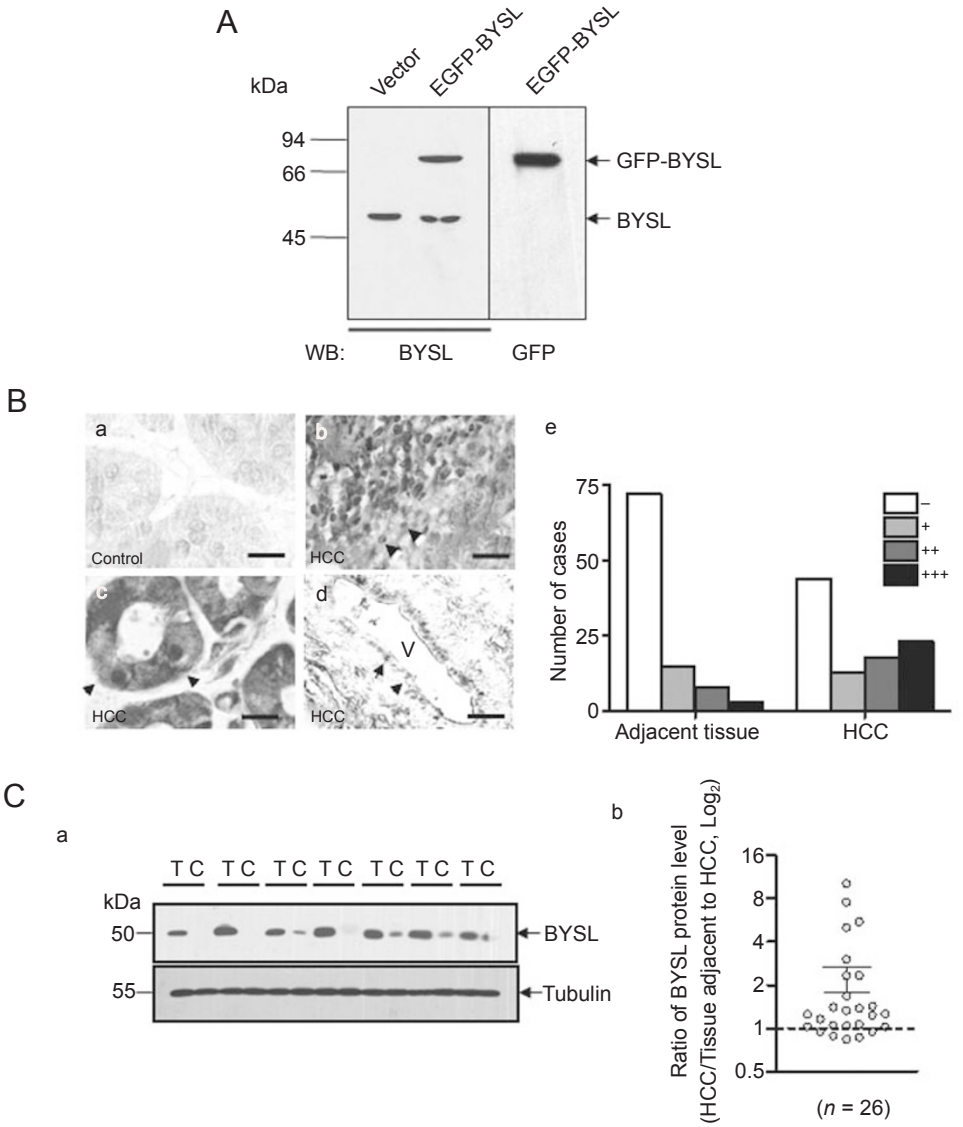

Figure 1 Characterization of BYSL expression in human hepatocellular carcinoma specimens. **(A)** Specificity of a polyclonal antibody against human BYSL (pAb). Lysates of HepG2 cells stably transfected with empty pEGFP-N1 vector or pEGFP-BYSL were analyzed by western blotting using a pAb against BYSL (aa 424-437). Expression and integrity of the exogenous GFP-BYSL fusion protein (~77 kDa) was verified using an anti-GFP antibody (middle and right lane, upper band) or the BYSL pAb. Endogenous BYSL (~50 kDa) was recognized by the pAb (left and middle lane, lower band). Exogenous GFP-BYSL was recognized by both antibodies. **(B)** BYSL expression in liver tissue of patients with HCC (panels b to d), and adjacent non-tumor tissue in corresponding patients (panel a). Immunohistochemistry with pAbs against BYSL was performed on formalin-fixed, paraffin-embedded sections. Both nuclear and cytoplasmic signals are observed in HCC patients (panels b and c). By contrast, a weak positive signal is present in adjacent tissue in some patients (panel a). Arrows in panel b indicate cells with nuclear BYSL immunosignals, whereas arrows in *c* indicate a pseudo-glandiform structure. Dense cytoplasmic staining is also observed in some specimens. Cytoplasmic BYSL immunosignals (indicated with arrows) in walls of blood vessels are detected in some specimens (panel d). Scale bars, a, b, 20 μm; c, 30 μm; d, 80 μm. Each pair of patient samples was classified separately as strongly positive (+++), intermediately positive (++), weakly positive (+) or negative (–), and the number of cases in each class is shown in panel e. **(C)** a, Western blot of BYSL protein in HCC patients using pAb against BYSL. T, tumor tissue; C, tissue adjacent to tumor in corresponding patient. α-tubulin expression served as a loading control (lower panel in a). b, Quantitation of BYSL protein levels normalized to tubulin, each compared to relevant adjacent non-tumor tissue. Data for each dot are mean values of three independent experiments (ratio of HCC/non-tumor adjacent tissue). Dashed line indicates control level (100%). Solid lines represent means ± SEM (n = 26). Data in **A** to **C** are representative of three independent experiments with similar results.

1B, panel e, the number of HCC cases with strong and intermediate immunoreactivity in tumor regions was much higher than that seen in adjacent tissues (41/98 versus 11/98), whereas the number of cases with weak or negative BYSL staining in HCC was significantly fewer than that in adjacent areas (57/98 versus 87/98). The elevated level of BYSL protein in the HCC specimens was confirmed by western blot analysis. On average, up to a 2.18-fold increase in BYSL proteins was observed in HCC specimens compared to that in controls (Figure 1C, panel b). To further characterize BYSL expression in HCC, a separate set of HCC and control specimens was analyzed for BYSL expression using real-time PCR. BYSL mRNA levels in HCC were increased from 1.5- to 3.0-fold compared to paired native liver tissue in five of eight sample pairs (Supplementary information, Figure S2). Together, these data indicate that BYSL is upregulated in HCC.

BYSL expression was also examined in clinical specimens of several other types of human cancer. BYSL immunoreactivity was observed in 6 of 10 pairs of invasive breast ductal carcinoma specimens, 1 of 4 pairs of intestine adenocarcinomas, 7 of 8 pairs of gastric adenocarcinoma, 1 of 2 pairs of cervical squamous cell carcinoma and all 5 pairs of esophageal squamous epithelioma in which nuclear and cytoplasmic signals were detectable (data not shown). These data further support our hypothesis that BYSL upregulation may be a general feature of human cancers.

BYSL is required for HCC cell growth in vitro and in vivo

To further investigate the role of BYSL in HCC tumorigenesis, we investigated the impact of suppressing BYSL expression on HCC cell growth using RNA interference (RNAi) methodology. Stable transfection of HepG2 and QSG-7701 cells with pSUPER-BYSL-RNAi (designated BYSL siRNA #1) resulted in marked reduction of BYSL levels to 42.15% ± 7.75% and 21.92% ± 5.13% of that found in controls, as revealed by western blot analysis (Supplementary information, Figure S3A). BYSL depletion in both HCC cell lines, HepG2 and QSG-7701, dramatically reduced their capacity to form colonies, as demonstrated by a significant decrease in the percentage of survived cell clones (47.8% of control in HepG2 cells and 25.9% in QSG-7701 cells) seen in colony-formation assays (Figure 2A, panels c and d). BYSL depletion also induced apoptosis and G2/M arrest of HepG2 cells, as revealed by fluorescence-activated cell sorter (FACS) analyses (Figure 2B). Consistently, BYSL knockdown markedly retarded cell growth, as manifested by a rightward shift of the growth curve shown in Figure 2C. These data suggest that BYSL is required for HCC growth and proliferation *in vitro*.

To determine whether BYSL is required for HCC formation *in vivo*, BYSL-depleted QSG-7701 cells were transplanted subcutaneously into nude mice and growth kinetics of HCC tumors were monitored. Seven weeks after inoculation, animals were sacrificed and the resulting tumors were examined. In mice receiving transplantation of BYSL siRNA-treated QSG-7701 cells, no tumor mass was detected in the flanks of mice, despite that small bumps in implantation sites were observed in the first week post implantation. By contrast, 100% of mice receiving QSG-7701 cells transfected with control siRNA developed tumors (1.88 ± 0.13 cm in diameter, $n = 3$) with an average volume of 1.5 cm^3 (Figure 2D). These results suggest that BYSL expression is necessary for tumor growth *in vivo*.

BYSL is localized to PR, NDF and PNBs during mitosis

To investigate cellular mechanisms underlying BYSL-siRNA-mediated suppression of HCC cell growth, we examined BYSL subcellular localization in mitotic cells based on the G2/M arrest of HepG2 cell line upon BYSL depletion (Figure 2B). As shown in Supplementary information, Figure S4 and in Figure 3A, exogenous BYSL-GFP expressed in HepG2 cells was localized to PR, as manifested by enrichment in regions surrounding chromosomes and co-localization with the nucleolar proteins nucleolin and B23 sequentially during mitosis. BYSL accumulation in PR began in prophase/prometaphase, through metaphase and persisted until anaphase. Beginning from anaphase, additional distinct BYSL foci were also observed in the cytoplasm. These foci were NDF, as they expressed B23 during anaphase and telophase (Figure 3A). These results suggest that BYSL is expressed in a dynamic pattern similar to other known nucleolar proteins during mitosis. Given that nucleologenesis occurs in anaphase and telophase through early G1, our findings, together with observations that BYSL localizes to subregions of nucleoli of interphase cells (Supplementary information, Figure S1), suggest that BYSL behaviors resemble other rRNA-processing proteins, such as B23, in human cells.

Next, we examined BYSL in the nucleologenesis PNB pathway in comparison with fibrillarin, nucleolin and B23. HepG2 cells were stably transfected with pEGFP-BYSL and examined by immunocytochemistry. In early telophase, fibrillarin was concentrated in PNBs while BYSL was absent (Figure 3B, panels a to d). Following recruitment of BYSL into PNBs, BYSL appeared in the newly assembled nucleolus (indicated by arrows in Figure 3B, panels e to h), which also contained nucleolin. In contrast, nucleolin, but not BYSL, remained in some

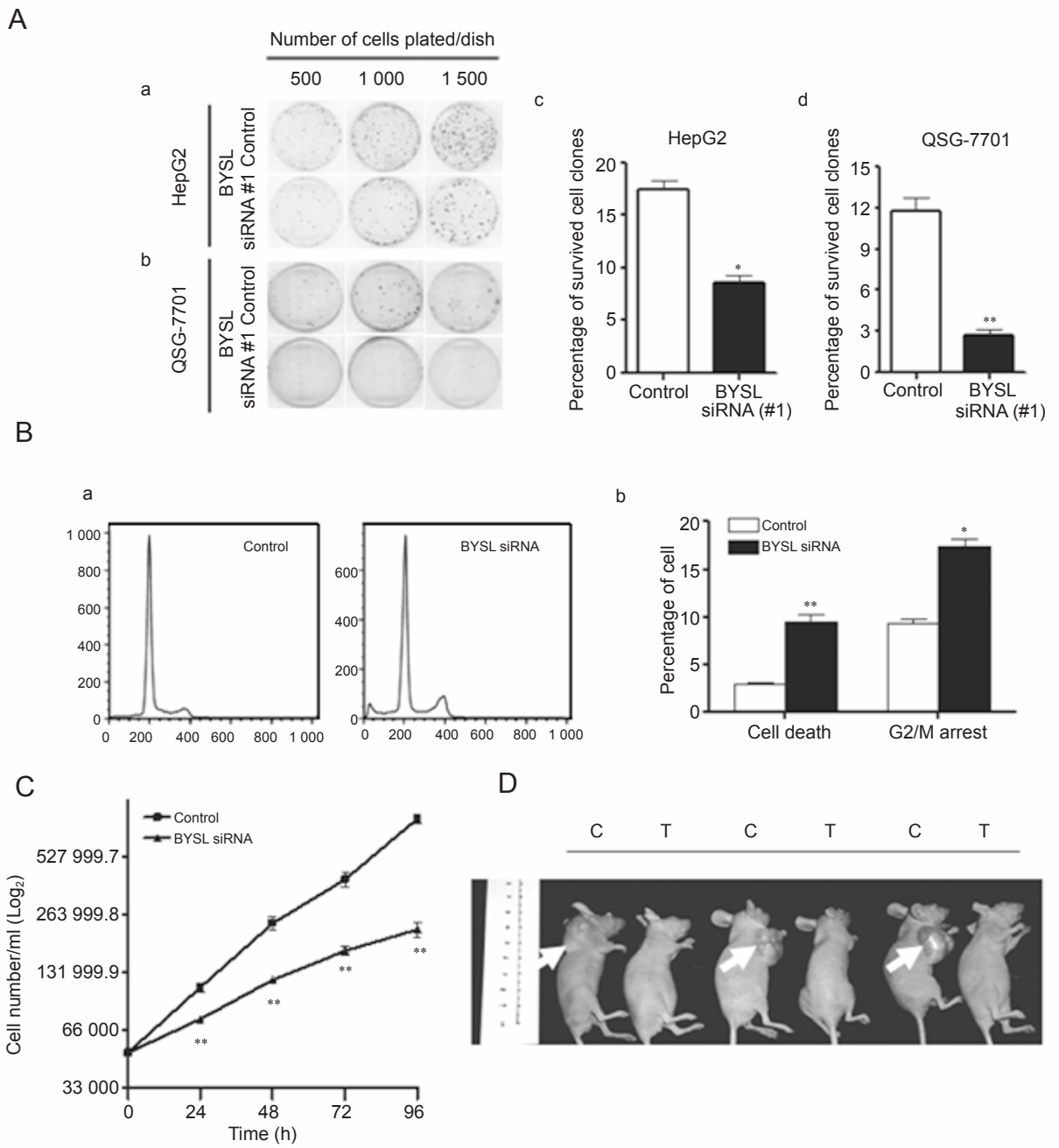

Figure 2 BYSL knockdown inhibits growth of human HCC cells *in vitro* and *in vivo*. **(A)** Colony-formation assays: HepG2 cells stably expressing BYSL siRNA show significantly reduced clone-forming capacity compared to controls plated at different cell densities (HepG2 cells, panels a and c; QSG-7701 cells, panels b and d). Quantitative data are shown in panels c and d. Data are from three independent experiments. **P* < 0.05 versus control, ***P* < 0.01 versus control. **(B)** BYSL knockdown by siRNA increases cell death and the number of cells arrested at G2/M phase (panel a). Data from three independent experiments are quantified in panel b. **P* < 0.05, ***P* < 0.01 versus control. **(C)** Stable expression of BYSL siRNA in QSG-7701 cells decreases cell growth relative to controls. QSG-7701 cells treated with or without BYSL siRNA were cultured and harvested at different intervals for counting. Cell growth curve shows the logarithm of the normalized number cells versus time. Data are of three independent experiments in triplicate with similar results. ***P* < 0.01 versus control. **(D)** BYSL knockdown reduced tumor-forming capacity of QSG-7701 cells *in vivo*. Mice received subcutaneous transplantation of BYSL siRNA-treated QSG-7701 cells (indicated by T) or control ones (indicated by C). Animals were sacrificed 7 weeks after transplantation. A total of 18 mice were used in the xenografting experiments. Experiments were repeated thrice with three mice per group with similar results. Arrows indicate tumor mass.

PNBs scattered around the newly assembled nucleolus (Figure 3B, panels e to h), suggesting that BYSL preferentially localizes to the nucleolus ahead of nucleolin. Conversely, B23 was recruited to the nucleolus later in the PNB pathway (Figure 3B, panels i to l). Here, BYSL participates in nucleologenesis earlier than nucleolin and B23, indicating different roles of BYSL in interphase r-RNA processing and the nucleologenesis process. Overall, we conclude that BYSL is associated with all structures, PR, NDFs and PNBs, which have roles in reassembly of the nucleolus following mitosis (Figure 3C).

BYSL depletion reduces NDF formation in mitotic phase and causes malformation of the nucleolus

To determine the role of BYSL in nucleologenesis, we performed loss-of-function analyses in HeLa cells transiently transfected with small RNAi. As shown in Supplementary information, Figure S3B, BYSL siRNA (#2) specifically knocked down endogenous BYSL expression 24 h after transfection without affecting levels of other known nucleolar proteins, such as Ubf (upstream binding transcription factor), fibrillarin, nucleolin and B23. We found that the number and distribution of NDF undergo dynamic changes with the progression of mitosis. Consistent with previous studies [35], NDF, marked by B23 immunostaining, first appeared in anaphase when condensed chromosomes began to separate from each other (Figure 4A, panel a). The number of NDF continued to increase with further chromosome separation (Figure 4A, panel c). When separated chromatin was de-condensed, NDF numbers began to decrease (Figure 4A, panel e). In contrast, following BYSL depletion, the number of NDF in mitotic HCC cells was reduced by 40.4% and the range of NDF distribution shrank compared to control cells (Figure 4B). These results indicate that BYSL may function during NDF formation and distribution.

To further investigate the role of BYSL in HCC cell nucleoli, we investigated the effect of BYSL RNAi on the expression of known nucleolar proteins using HepG2 cells stably transfected with BYSL siRNA. We used Ubf to mark Pol I transcription sites [36]. Fibrillarin served as a marker of the dense fibrillar compartment (DFC) rich in nascent pre-rRNAs [37]. Thus, Ubf, fibrillarin, nucleolin and B23 represent distinct aspects of nucleolus activity from pre-rRNA transcription to late events of rRNA processing. Compared to controls, BYSL depletion markedly reduced the number of active NORs in HepG2 cells, as revealed by immunostaining. Small Ubf-positive foci were converted to larger condensed spots when BYSL was suppressed (Figure 4C, panels a and b), suggesting a reduction in active transcription sites in the nucleolus. Similarly, fibrillarin-enriched early rRNA-processing regions were also disrupted and merged forming larger, more condensed structures (Figure 4C, panels c and d). Nucleolin immunostaining showed that the nucleolin-containing perinucleolar compartment became more centralized in nucleoli (Figure 4C, panels e and f). Moreover, B23 distribution in nucleoli was markedly altered, with the appearance of numerous small particles in the nucleoplasm like PNB in interphase cells (Figure 4C, panels g and h). Taken together, these results suggest that BYSL depletion disrupts both early phases of nucleolus assembly such as NDF formation and late steps in the PNB pathway.

BYSL depletion reduces HCC cell tolerance to serum starvation

To further characterize its role and mechanism in HCC cell growth, we asked whether BYSL functions in serum-starvation-induced apoptosis in HepG2 cells. BYSL suppression significantly decreased the viability of HepG2 cells maintained in culture following reduction of serum compared with controls (Figure 5A**).** Cell growth suppression induced by BYSL RNAi was further characterized using FACS (Figure 5C). The percentage of apoptotic cells in BYSL-depleted HepG2 cells was dramatically increased in cultures with either complete or partial removal of serum compared with control cultures. To determine how serum starvation increased apoptosis of BYSL-depleted cells, we examined BYSL distribution using immunocytochemistry upon serum deprivation. Comparing to normal control cells with complete culture medium, the number of BYSL-positive foci in nucleoli was remarkably reduced from 4-7 foci to 1-2 foci per cell, 1 day after serum deprivation. This reduction was accompanied by diffuse nucleolar BYSL and nucleolin immunosignals (Figure 5B). These abnormalities became more severe on day 3, suggesting that the nuclear machinery was disrupted following serum starvation. In contrast, in the absence of serum for 24 h, HepG2 cells still maintained normal PR structure (data not shown), but no NDF were formed (Figure 6B, left panels). BYSL protein appeared dispersed in the cytoplasm outside the dividing nucleus and accumulated as small granules resembling NDF structure (indicated with arrows) but lacking B23-positive signals. This indicated a BYSL function in NDF formation distinct from that of B23. In HepG2 cells treated with BYSL siRNA (Figure 6B, middle panels), all NDF-like structure seems dissolved and PR structure was abnormal. Without BYSL protein, HCC cells subjected to serum starvation underwent significant apoptosis, as revealed by Hoechst staining; the dying cells crowded together compared to the rare apoptotic ones in normal BYSL-level group (Supplementary

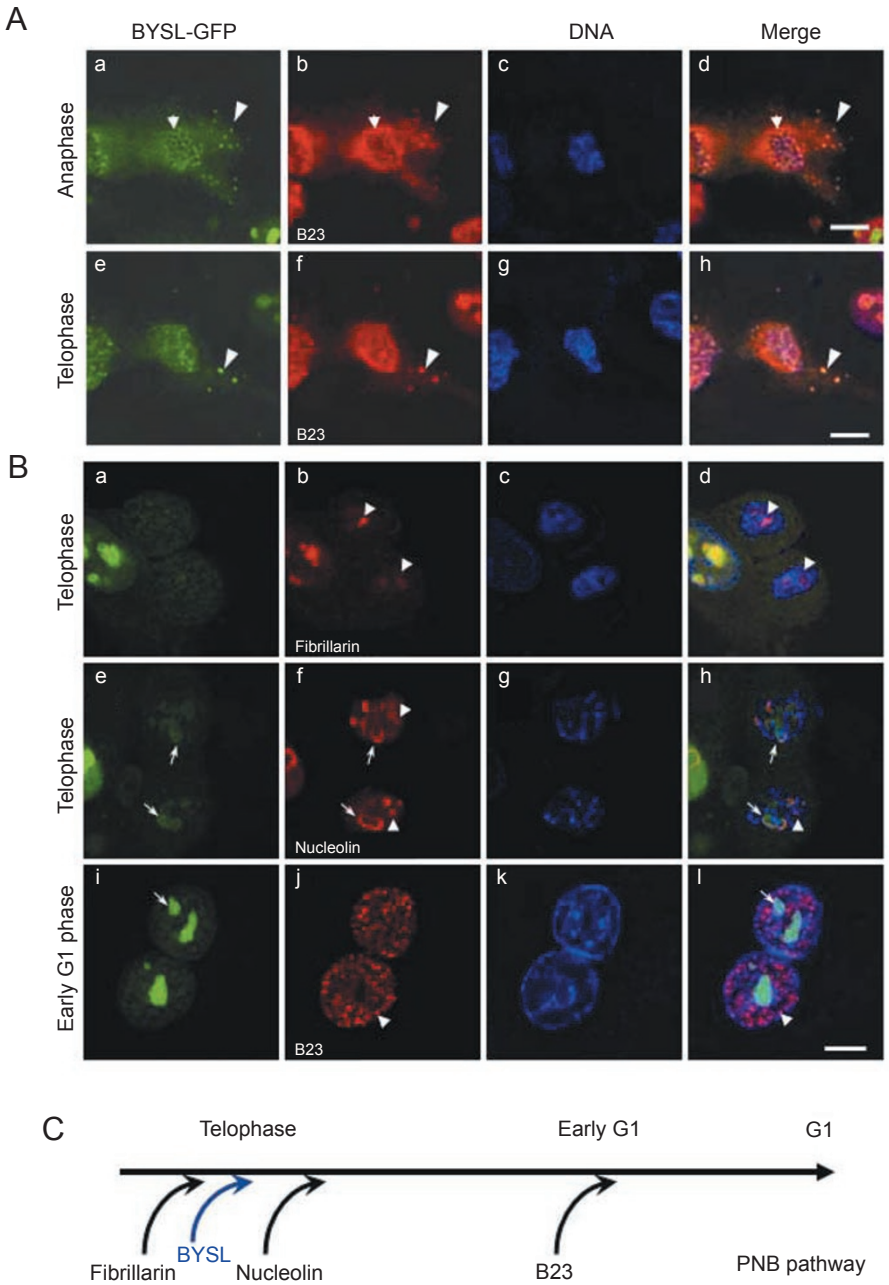

Figure 3 Subcellular localization of BYSL in mitosis. **(A)** HepG2 cells were stably transfected with pEGFP-BYSL, and stained with nucleolin and B23 antibodies. The perichromosomal layer, indicated by arrows, is present in prometaphase, metaphase (Supplementary information, Figure S4) and anaphase (panels a to d). Nucleolus-derived foci containing BYSL, indicated by arrowheads, are observed in anaphase (panels a to d) and telophase (panels e to h). Left panel, BYSL-eGFP is in green, B23 (panels b and f) is in red and DNA stained with Hoechst 33258 is in blue. Scale bar, 5 μm. **(B)** BYSL kinetics relative to other nucleolar proteins during nucleolus formation. HepG2 cells stably transfected with BYSL-GFP were double-stained using antibodies to nucleolar proteins. Images show comparison of BYSL with fibrillarin (panels a to d) or nucleolin (panels e to h). By contrast, BYSL does not colocalize with B23 (panels i to l). Arrowheads indicate PNBs, whereas arrows indicate newly assembled nucleoli. When fibrillarin is recruited to nucleoli, BYSL remains in PNBs (panels a to d). After BYSL is recruited into nucleoli, nucleolin (panels e to h) and B23 (panels i to l) remain in PNBs. With cell cycle progression from late telophase to early G1, colocalized immunosignals increase in the nucleolus. Scale bar, 5 μm. **(C)** Kinetics of translocation of nucleolar proteins including BYSL during nucleologenesis (modified from Savino *et al.* [54]). Data shown in **A** to **B** represent at least three independent experiments with similar results.

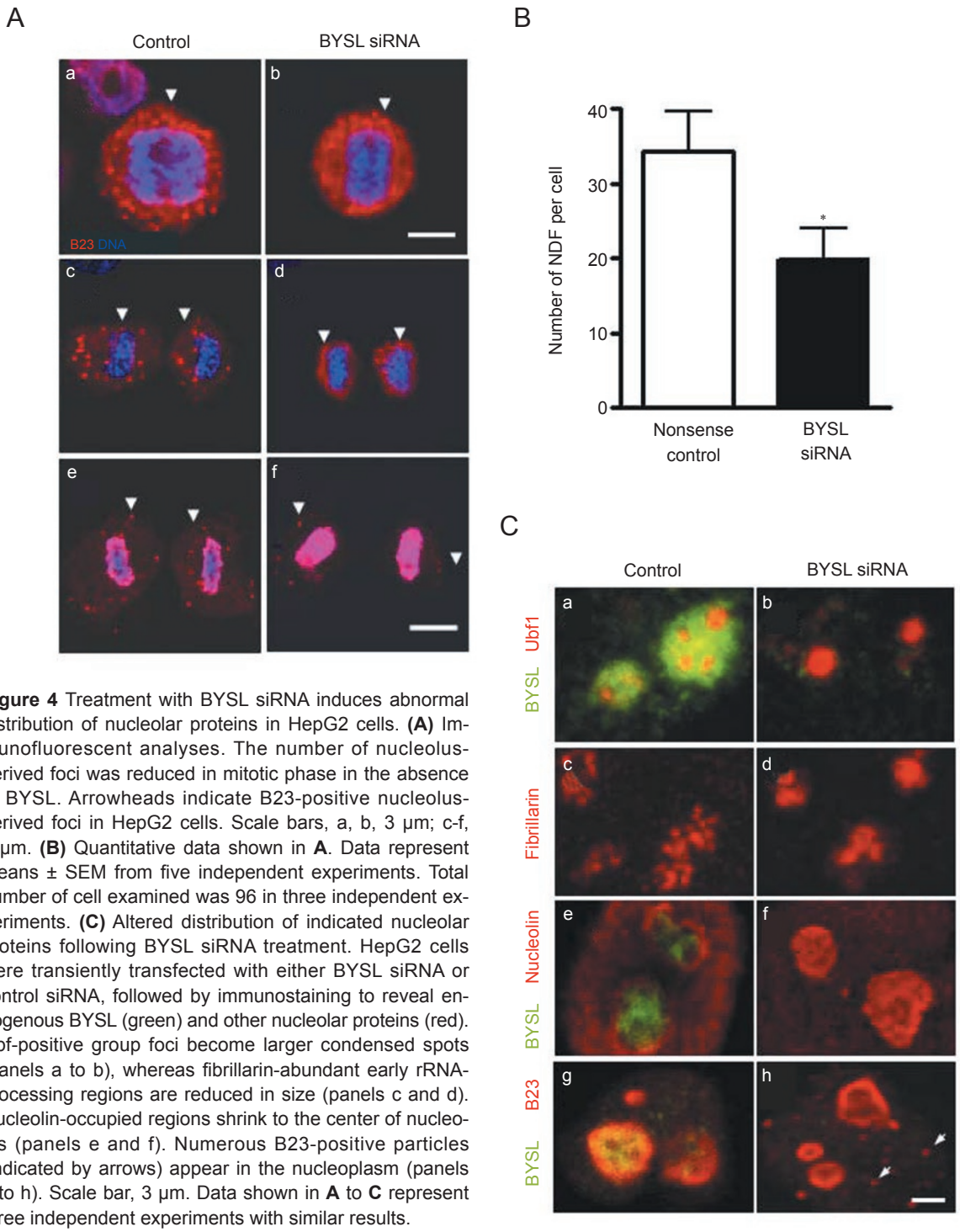

Figure 4 Treatment with BYSL siRNA induces abnormal distribution of nucleolar proteins in HepG2 cells. **(A)** Immunofluorescent analyses. The number of nucleolus-derived foci was reduced in mitotic phase in the absence of BYSL. Arrowheads indicate B23-positive nucleolus-derived foci in HepG2 cells. Scale bars, a, b, 3 μm; c-f, 5 μm. **(B)** Quantitative data shown in **A**. Data represent means ± SEM from five independent experiments. Total number of cell examined was 96 in three independent experiments. **(C)** Altered distribution of indicated nucleolar proteins following BYSL siRNA treatment. HepG2 cells were transiently transfected with either BYSL siRNA or control siRNA, followed by immunostaining to reveal endogenous BYSL (green) and other nucleolar proteins (red). Ubf-positive group foci become larger condensed spots (panels a to b), whereas fibrillarin-abundant early rRNA-processing regions are reduced in size (panels c and d). Nucleolin-occupied regions shrink to the center of nucleolus (panels e and f). Numerous B23-positive particles (indicated by arrows) appear in the nucleoplasm (panels g to h). Scale bar, 3 μm. Data shown in **A** to **C** represent three independent experiments with similar results.

information, Figure S5). Further observation showed that many BYSL-depleted cancer cells died in couple in serum starvation condition, indicating that cells with failed nucleogenesis died at the end of mitosis (Figure 6B, right panels and Supplementary information, Figure S5). In interphase cells, following treatment with BYSL siRNA in combination with serum deprivation for 24 h, expression of nucleolin in nucleoli was altered, as evidenced by

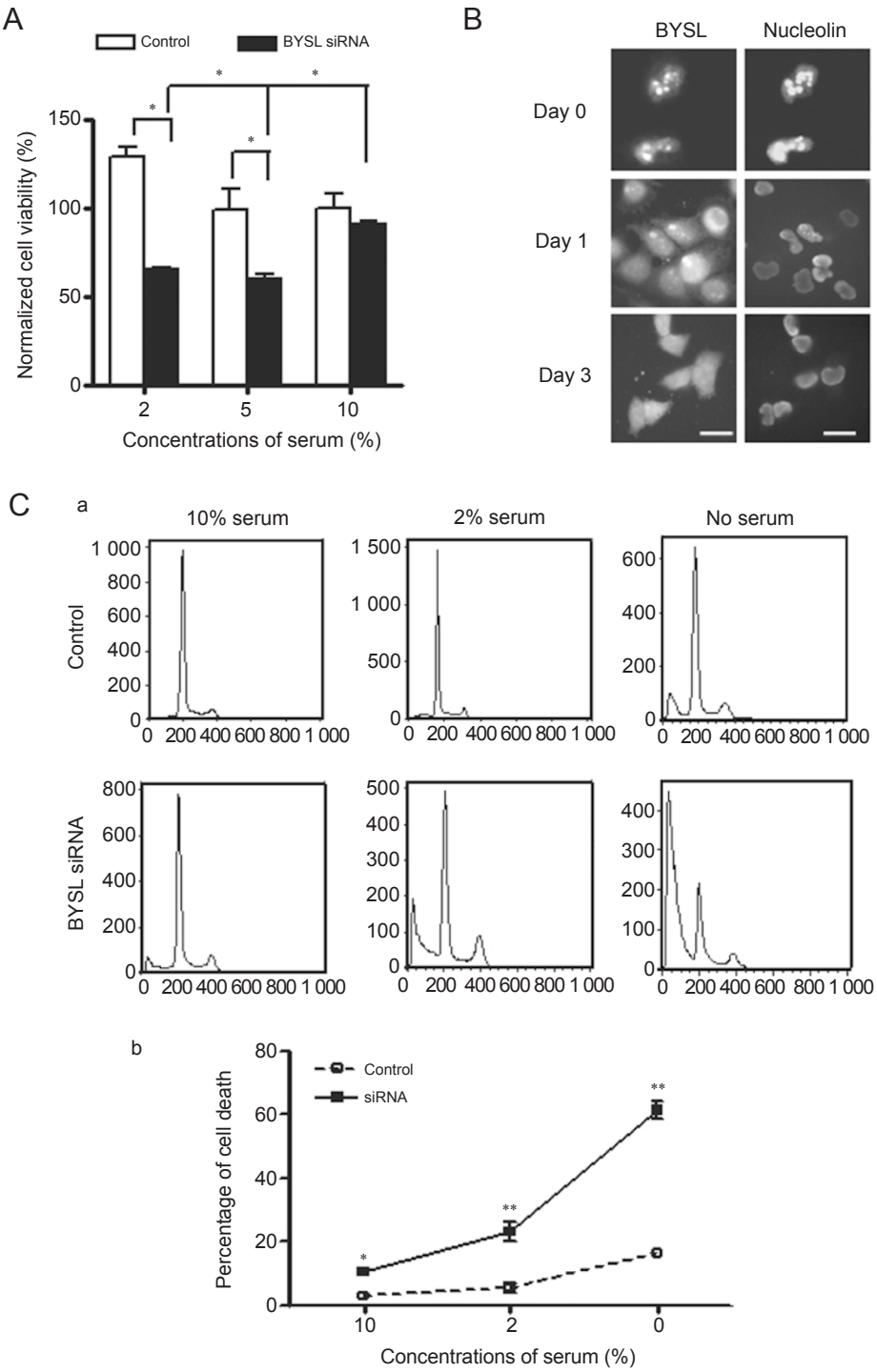

Figure 5 BYSL siRNA reduces resistance of hepatocarcinoma cells to serum starvation. **(A)** HepG2 cells were treated with or without BYSL siRNA and maintained in the presence of different concentrations of serum. Their viabilities were assayed using MTT-based cell viability assay on day 3 *in vitro*. Data represent means ± SEM of three independent experiments in triplicate. $^{**}P < 0.01$ versus control. **(B)** Immunofluorescence. Serum starvation alters nucleolar localization of BYSL and nucleolin. At 72 h after serum starvation, endogenous BYSL and nucleolin become dispersed in the cytoplasm. Scale bar, 5 μm. Data represent three independent experiments with similar results. **(C)** FACS analyses. Cells were treated with BYSL siRNA and maintained in the presence of indicated concentrations of serum for 72 h. The percentage of apoptotic cells was determined using FACS analyses (panel a). Panel b, Quantitation of apoptosis by FACS analyses as shown in panel a. Data are means ± SEM of three independent experiments. $^{*}P < 0.05$, $^{**}P < 0.01$ versus control.

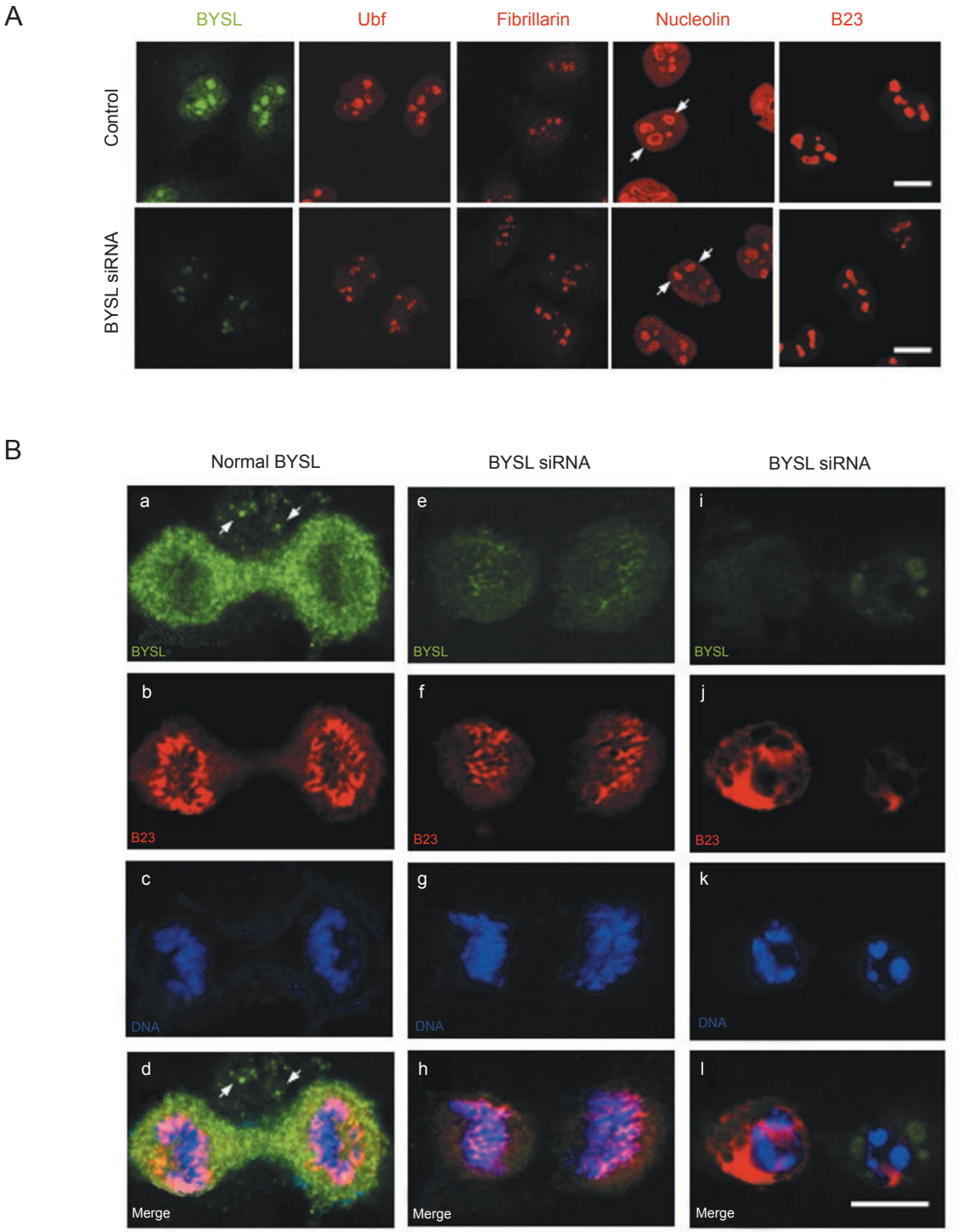

Figure 6 BYSL siRNA alters nucleolar protein distribution, disturbs NDF formation and leads to cell death in serum starvation condition. **(A)** Following treatment with BYSL siRNA, serum starvation alters nucleolar expression of nucleolin and B23. At 24 h after serum starvation, BYSL knockdown promotes loss of endogenous BYSL. Nucleolin becomes dispersed in nucleoli (indicated with arrows). Scale bar, 8 μm. **(B)** In the absence of serum for 24 h, NDF failed to form in HepG2 cells (left panels). BYSL-positive signals appeared dispersed to the cytoplasm outside the dividing nucleus and accumulated to small granules resembling NDF structure (white arrows) but without B23-positive signals. While in HepG2 cells treated with BYSL siRNA (middle panels), all NDF-like structure seems dissolved. Cell death following BYSL depletion is coupled with serum starvation condition (right panels). Scale bar, 5 μm.

the fact that nucleolin-containing foci became dispersed and nucleolin immunosignals were less intense compared to controls (Figure 6A). Moreover, B23 immunosignals were reduced, whereas Ubf and fibrillarin were not affected (Figure 6A). These data suggest that BYSL is necessary for tolerance to serum starvation in HCC cells. Loss of BYSL sensitized HCC cells to serum starvation-induced apoptosis especially in mitotic phase. Abnormal nucleologensis was likely the initial cause of cell death in serum-deprived HCC cell lines.

Discussion

In the present study, we showed that BYSL is crucial for cell growth and HCC tumor formation *in vitro* and *in vivo*. Recent studies have shown that BYSL is expressed at higher levels in embryonic stem cells, HeLa and 293T cell lines [15, 16, 19]. Here, we reported for the first time that BYSL expression is upregulated in human HCC specimens. A previous study mentioned that BYSL inhibited cancer cell proliferation *in vitro* [15]. Our findings showed that BYSL knockdown greatly suppresses HCC cell growth *in vitro* and tumor formation *in vivo*. We also observed BYSL upregulation in other cancer specimens, such as breast cancer, intestinal adenocarcinomas and gastric adenocarcinoma. Moreover, the BYSL gene is frequently amplified in diffuse large B-cell lymphoma [38]. Overall, these observations suggest that BYSL upregulation may be a general feature of human cancers and crucial for tumor formation. BYSL is not a widely expressed gene in adult human tissue through both northern blot and immunohistology analysis in various human tissues [39]. The lack of BYSL protein leads to G2/M arrest and cell death at the end of mitosis in cancer cells, indicating that BYSL is more required in continual cell division. Given that c-myc binds to the BYSL promoter in a B-cell line [20], is expressed highly and plays a critical role in both cancer and preimplantation mammalian embryo development [40, 41], BYSL is likely an important component of the machinery activated by c-myc and a new marker in cancer.

In addition to its role in 18S rRNA processing and 40S ribosomal subunit biogenesis, which is conserved from yeast to human [16, 17], we report novel functions of BYSL in nucleolar assembly in human cancer cells. PNBs have been shown to originate from the PR [42], whereas NDF also contribute to nucleoli reassembly by supplying components to PNBs when NDF disappear during telophase [5]. Our data show that all three structures, PR, NDF and PNBs, contain BYSL protein (Figure 3), suggesting that BYSL is intimately associated with nucleologenesis at the end of mitosis. In higher eukaryotic cells, dynamic assembly of nucleoli is an important event at the exit of mitosis. The assembly of the nucleolus requires relocalization and reactivation of the pre-rRNA-processing machinery. The detailed mechanisms of the assembly are still poorly understood [43]. Here, we show that nucleolar localization of multiple factors crucial for nucleologenesis, including Ubf, fibrillarin, nucleolin and B23, is disrupted in BYSL-knockdown cells (Figure 4C). Thus, BYSL knockdown may impair nucleologenesis by incorrect localization or inactivation of these factors, leading to retardation of HCC cell growth. This is consistent with a previous study showing that loss of function of several proteins, including cyclin-dependent kinases [44], induced similar defects, suggesting their potential interactions.

Our study also suggests that BYSL is likely to be involved in the maintenance of NDF/PNB integrity. We found that BYSL is moved back to the nucleoli very early in the PNB pathway just after fibrillarin, but before nucleolin and B23 in mitotic cells. In assembled nucleus, neuleolar proteins are expressed in distinct regions of the nucleoli. It is known that Ubf is expressed in the fibrillar centers. Fibrillarin localizes in DFC and B23 occupies the granular component. By contrast, BYSL is localized in all three subregions (Figure 6C). These results suggest extensive roles of BYSL in nucleolar machinery. Loss of function through BYSL siRNA could deregulate this sequence and impair coordinate expression of these factors. Indeed, expanded distribution of fibrillarin and nucleolin in nucleoli was observed in cells treated with BYSL siRNA (Figure 4C). BYSL depletion also reduced NDF formation (Figure 4). Same knockdown treatment distorts nuclear shape in PNB formation stage indicating less healthy cells exiting mitosis (Supplementary information, Figure S6). B23, which was expressed later in the PNB pathway than BYSL, showed markedly altered nuclear distribution in BYSL-depleted interphase cells, with the appearance of numerous small particles in the nucleoplasm like PNB (Figure 4C, panels g and h), indicating incompleted PNB pathway without BYSL. Defects in nucleolar assembly following BYSL depletion indicate that BYSL regulates nucleolar activity at multiple steps involving PR, NDF and PNB formation and is essential for sthenic cancer cell proliferation.

Lastly, we found that BYSL is also present in the cytoplasm in human HCC. This observation agrees with the previous studies reporting BYSL in nuclei of yeast and mouse ES cells, while only small amounts of BYSL/ENP1 were cytoplasmic in HeLa cells and yeast [17, 18]. Interestingly, BYSL promotes cell adhesion of trophoblasts by forming a complex with trophinin and tastin [39, 45], thus mediating embryo implantation which is

accompanied by rapid cellular invasion and proliferation [39, 46, 47]. It is likely that cytoplasmic activity of BYSL is important in cancer cell metastasis. Indeed, trophinin, one of BYSL-interacting proteins, has been found to promote metastasis of testicular germ cell tumor [48]. *Tastin*, another BYSL-interacting protein, is required for bipolar spindle assembly and centrosome integrity during mitosis, and is suggested to be a tumor-associated antigen in prostate cancer and perhaps other cancers [49]. Given that BYSL plays multiple roles, it is conceivable that BYSL knockdown dramatically impairs HCC cell growth *in vitro* and *in vivo*. Our observations suggest that BYSL could be a potential target for cancer therapy, as its suppression could impair mitosis, thereby inhibiting abnormal cell growth and survival.

In summary, our data demonstrate that BYSL plays an important role in rapid growth of HCC cells. BYSL mediates NDF and PNB formation, which ultimately contributes to nucleolar assembly during cell division. Inhibiting BYSL-mediated nucleologenesis in mitotic cells may be an effective means to disrupt tumorigenesis. Our results also provide a new basis for developing novel approaches in HCC cancer therapy.

Materials and Methods

Human HCC specimens

Paraffin-embedded tumor specimen sections (5-μm thick) from 98 HCC patients and 34 biopsies were obtained from multiple hospitals in the Shanghai and Jiangsu regions of China following local ethical considerations. Patients received curative resection for primary HCC. All samples were diagnosed as HCC and graded as stages III-IV. Paraffin-embedded tumor specimen sections were immunostained. A total of 34 biopsies containing tumor and adjacent tissue were used for either western blot (26 biopsies) or real-time PCR (8 biopsies) analysis.

Antibodies

Antibodies used were an anti-Ubf antibody (1:500, Santa Cruz Biotech., Santa Cruz, CA, USA), anti-fibrillarin antibody (1:500, Santa Cruz Biotech.), anti-nucleolin antibody (1:500, Santa Cruz Biotech.), anti-B23 antibody (1:500, Sigma-Aldrich, St. Louis, MO, USA) and anti-GFP antibody (1:500, Santa Cruz Biotech.). Rabbit anti-human BYSL pAb (1:1 000) was raised against the synthetic peptide AVPRDVEDVPITVE (aa 424-437) based on C-terminal sequence of human BYSL (GenBank accession number NM_004053).

Immunohistochemical analysis of liver tissue sections from HCC patients

Immunohistochemical staining of BYSL was performed on formalin-fixed, paraffin-embedded sections from 98 sample blocks using the standard avidin-biotin complex method. Briefly, enzymatic antigen retrieval was performed using 0.1% trypsin at 37 °C for 15 min. After blocking, sections were incubated in BYSL antibodies overnight (1:1 000), followed by incubation in secondary antibodies and further incubation with the streptavidin-biotin complex (Vectastain Elite ABC Kit; Vector Laboratories, Burlingame, CA, USA). Reactivity was developed in chromogen DAB solution. The sections were then dehydrated and mounted. Brown cellular staining was considered positive labeling. Sections were observed under a light microscope, and the degree of BYSL expression was scored and assessed based on the percentage and staining intensity of positive cells. Tumor-containing areas and adjacent tissue were classified as strongly positive (+++) (70% cells staining positive), intermediately positive (++), weakly positive (+) or negative (–).

Quantitative RT-PCR analysis

HCC tissue and adjacent tissue were homogenized and total RNA was extracted using TRIzol reagent (Invitrogen, Carlsbad, CA, USA). Single-strand cDNA was synthesized from 1 μg total RNA using Superscript II Reverse Transcriptase (Invitrogen). Real-time PCR analysis was performed for 40 cycles to amplify a 140-bp BYSL fragment (nt 1 332-1 471) using SYBR Premix Ex Taq™ (Takara Biotechnology, China) and an ABI Prism 7000 amplifier (Applied Biosystems, UK). Beta-actin served as an internal control. Primers: BYSL: forward, 5′-GGA ATA CAG CGG TGC CAA CA-3′ and reverse, 5′-GCC ACA GCA CAG GCA GTT CA-3′; β-actin: forward, 5′-TTG CGT TAC ACC CTT TCT TGA CA-3′ and reverse, 5′-TCA CCT TCA CCG TTC CAG TTT T-3′. The reaction was carried out in triplicate for each specimen at least thrice.

Plasmid construction

Full-length cDNAs encoding human BYSL were purchased from Invitrogen and subcloned into the *EcoR*I and *BamH*I restriction sites of pEGFP-C1 vector (BD Biosciences Clontech, Palo Alto, CA, USA) to add an N-terminal GFP tag.

Cell culture and transfection

HeLa, NIH-3T3, the hepatocarcinoma cell line HepG2, as well as the hepatocarcinoma cell line QSG-7701 were used. This latter line was derived from liver carcinoma peripheral tissue taken from a 35-year-old woman [50] and has been used in recent years for HCC studies [28, 51, 52]. Cells were grown in Dulbecco's modified Eagle medium (DMEM, Invitrogen) supplemented with 10% (v/v) heat-inactivated fetal bovine serum, 2 mM glutamine, 100 U/ml penicillin and 0.1 μg/ml streptomycin at 37 °C in an atmosphere of 5% CO_2. HeLa, HepG2 and QSG-7701 cells were transfected using Lipofectamine 2000 transfection reagent (Invitrogen). To obtain clones stably expressing BYSL-eGFP or BYSL siRNA, transfected HepG2 or QSG-7701 cells were treated with G418, and GFP-positive clones were identified by western blotting. In some experiments, cells were harvested at 24 h intervals for 96 h, and cell numbers were determined using a Coulter counter (Beckman, Fullerton, CA, USA).

RNAi

Two BYSL siRNAs were used. For *in vivo* studies, a pSUPER vector-based construct encoding BYSL siRNA and EGFP (designated BYSL siRNA #1) to allow tracking of transfected cells was prepared according to the manufacturer's protocols (OligoEngine). Briefly, a BYSL target sequence $_{519}$5′-GAA GCA GAC AGA GGT GGA G-3′$_{538}$ was selected. Two complementary oligonucleotides, 5′-GAT CCC CGA AGC AGA CAG AGG TGG AGT TCA AGA

GAC TCC ACC TCT GTC TGC TTC TTT TTA-3′ and 5′-AGC TTA AAA AGA AGC AGA CAG AGG TGG AGT CTC TTG AAC TCC ACC TCT GTC TGC TTC GGG-3′ were synthesized. After annealing, the resulting products were cloned into the *Bgl*II and *Hind*III sites of pSUPER to generate the siRNA duplex. siRNA targeting $_{1135}$5′-CGA CTC AAC TTC CAT CTC T-3′$_{1153}$ (designated BYSL siRNA #2) was synthesized (GeneChem, Shanghai, China) and transfected into HepG2 cells using TransMessenger Transfection Reagent (QIAGEN, Germany). HepG2 and QSG-7701 cells were transfected using either Nucleofector™ (Amaxa, Cologne, Germany) or Lipofectamine™ 2000 (Invitrogen) according to the manufacturers' protocols. The efficiency and specificity of siRNA targeting to BYSL was determined by western blot analysis. A mock construct (target sequence: UUC UCC GAA CGU GUC ACG UTT) that had no effect on BYSL expression served as a control.

Western blotting assay

Briefly, total proteins were collected in RIPA buffer (20 mM Tris-HCl, pH 7.4, 0.1% SDS, 1% NP-40, 1% sodium deoxycholate and protease inhibitor cocktail) from cell or tissue samples. Whole-cell or tissue lysates were separated by SDS-polyacrylamide gel electrophoresis and transferred to nitrocellulose membranes. Immunoblots were incubated with primary antibodies followed by peroxidase-linked secondary antibodies. Band intensities were visualized by SuperSignal West Pico Chemilluminescent substrate (Pierce, Rockford, IL). In some cases, bands were digitized and optical densities were analyzed using ImageMaster 2D Platinum (v.5.0, Amersham Biosciences Piscataway, NJ, USA).

Immunofluorescence, confocal microscopy and image analysis

For most immunofluorescence experiments, cells were grown on coverslips and fixed with 4% paraformaldehyde for 30 min. After treatment with 1% Triton X-100 in PBS, cells were incubated in PBS containing 4% goat serum albumin for 1 h. To visualize NDF, cells were fixed as described by Dundr *et al.* [5] with modifications. Cells on coverslips were fixed with 4% paraformaldehyde and permeabilized with 0.2% Triton X-100 in PBS for 5 min on ice and then washed extensively with PBS. Cells were incubated with primary antibodies overnight at 4 °C, followed by incubation with appropriate secondary antibodies. Cells were imaged using either a cooled CCD SPOT II (Diagnostic Instruments, MI, USA) on a microscope (BX51) or a confocal laser-scanning microscope (TCS SP2, Leica, Bensheim, Germany). Optical sections were scanned at 0.2-0.5 μm intervals. Z stack images were then formed by maximal projection. Data were obtained and processed using Adobe Photoshop 7.0 software (Adobe Systems).

Clone-forming assay

Cells were cultured for 4 weeks and stained with hematoxylin. Digital photographs of plates were taken and the number of clones containing at least 50 cells was determined using 2D ImageMaster 2D Platinum software (Amersham Biosciences). The clone-forming rate of tumor cells was calculated as: (the number of clones identified/ the number of cells seeded) ×100%.

Cell viability assay (MTT-based method)

The assay was performed as described previously [53], with some modifications. Cells were incubated with 0.25 mg/ml MTT (Sigma, USA) for 48 h at 37 °C and the reaction stopped by adding a solution containing 50% dimethyl-formamide and 20% sodium dodecyl sulfate (pH 4.8). The amount of MTT formazan product was determined by measuring absorbance with a microplate reader at a test wavelength of 570 nm. A growth curve of tumor cells was generated every 2 days using the MTT assay over a period of 10 days (n = 6). For serum starvation experiments, cells were surveyed 48 h in innutritious culture.

FACS analysis

HCC cell lines were fixed, stained with propidium iodide and analyzed for DNA content on a FACSca flow cytometer using CellQuest software (BD Biosciences).

Tumor xenografts in Balb/c nude mice

Mice were maintained according to guidelines of the Ethical Committee for animal use at the Shanghai Institutes for Biological Sciences. 6-week-old male athymic nude mice (Balb/c nu/nu) obtained from an animal house (SIBS, Chinese Academy of Sciences) were caged in groups with free access to sterilized food and autoclaved water, and kept in a temperature-controlled environment on a 12 h light/dark cycle. A suspension of QSG-7701 cells stably expressing BYSL siRNA (1×10^7) was injected subcutaneously into the back of each mouse. Animals were maintained for 50 days before they were sacrificed.

Statistical analysis

Statistical analysis was carried out using statistical software (GraphPad Prism v4.0, GraphPad Software Inc.). The control group was compared with different treatment groups using one- or two-way ANOVA followed by Dunnet's test. Differences were considered significant when P values were < 0.05.

Acknowledgments

We thank Dr ZJ Chen of Institute of Biochemistry and Cell Biology, Shanghai Institutes for Biological Sciences, Chinese Academy of Sciences for kindly providing HCC samples and Dr YZ Wang of Institute of Neuroscience, Shanghai Institutes for Biological Science, Chinese Academy of Sciences for the nucleolin antibody. We also thank Dr G Chen of Shanghai Chest Hospital for help in examining human pathological specimens. This work was supported by grants from the Chinese Academy of Sciences, National Natural Science Foundation of China (Nos. 30525041 and 30623003) and State Key Program for Basic Research of China (No. 2006CB500704).

References

1 Leong TY, Leong AS. Epidemiology and carcinogenesis of hepatocellular carcinoma. *HPB (Oxford)* 2005; **7**:5-15.
2 Kodousek R, Dusek J. Demonstration of the nucleolar organizer region by silver staining (AgNOR method) in research and in histopathological practice. *Acta Univ Palacki Olomuc Fac Med* 1991; **131**:9-37.
3 Derenzini M, Sirri V, Trere D, Ochs RL. The quantity of nucleolar proteins nucleolin and protein B23 is related to cell doubling time in human cancer cells. *Lab Invest* 1995; **73**:497-502.

4 Sirri V, Roussel P, Hernandez-Verdun D. The AgNOR proteins: qualitative and quantitative changes during the cell cycle. *Micron* 2000; **31**:121-126.
5 Dundr M, Misteli T, Olson MO. The dynamics of postmitotic reassembly of the nucleolus. *J Cell Biol* 2000; **150**:433-446.
6 Yun JP, Miao J, Chen GG, *et al*. Increased expression of nucleophosmin/B23 in hepatocellular carcinoma and correlation with clinicopathological parameters. *Br J Cancer* 2007; **96**:477-484.
7 Storck S, Shukla M, Dimitrov S, Bouvet P. Functions of the histone chaperone nucleolin in diseases. *Subcell Biochem* 2007; **41**:125-144.
8 Kondoh N, Shuda M, Tanaka K, *et al.* Enhanced expression of S8, L12, L23a, L27 and L30 ribosomal protein mRNAs in human hepatocellular carcinoma. *Anticancer Res* 2001; **21**:2429-2433.
9 Bassoe CF, Bruserud O, Pryme IF, Vedeler A. Ribosomal proteins sustain morphology, function and phenotype in acute myeloid leukemia blasts. *Leuk Res* 1998; **22**:329-339.
10 Alon U, Barkai N, Notterman DA, *et al.* Broad patterns of gene expression revealed by clustering analysis of tumor and normal colon tissues probed by oligonucleotide arrays. *Proc Natl Acad Sci USA* 1999; **96**:6745-6750.
11 Ferrari S, Manfredini R, Tagliafico E, *et al.* Noncoordinated expression of S6, S11, and S14 ribosomal protein genes in leukemic blast cells. *Cancer Res* 1990; **50**:5825-5828.
12 Ruggero D, Grisendi S, Piazza F, *et al.* Dyskeratosis congenita and cancer in mice deficient in ribosomal RNA modification. *Science* 2003; **299**:259-262.
13 Ruggero D, Pandolfi PP. Does the ribosome translate cancer? *Nat Rev Cancer* 2003; **3**:179-192.
14 Willig TN, Draptchinskaia N, Dianzani I, *et al.* Mutations in ribosomal protein S19 gene and diamond blackfan anemia: wide variations in phenotypic expression. *Blood* 1999; **94**:4294-4306.
15 Miyoshi M, Okajima T, Matsuda T, Fukuda MN, Nadano D. Bystin in human cancer cells: intracellular localization and function in ribosome biogenesis. *Biochem J* 2007; **404**:373-381.
16 Adachi K, Soeta-Saneyoshi C, Sagara H, Iwakura Y. A crucial role of Bysl in mammalian preimplantation development as an integral factor for 40S ribosome biogenesis. *Mol Cell Biol* 2007; **27**:2202-2214.
17 Chen W, Bucaria J, Band DA, Sutton A, Sternglanz R. Enp1, a yeast protein associated with U3 and U14 snoRNAs, is required for pre-rRNA processing and 40S subunit synthesis. *Nucleic Acids Res* 2003; **31**:690-699.
18 Schafer T, Strauss D, Petfalski E, Tollervey D, Hurt E. The path from nucleolar 90S to cytoplasmic 40S pre-ribosomes. *EMBO J* 2003; **22**:1370-1380.
19 Aoki R, Suzuki N, Paria BC, *et al.* The Bysl gene product, bystin, is essential for survival of mouse embryos. *FEBS Lett* 2006; **580**:6062-6068.
20 Basso K, Margolin AA, Stolovitzky G, *et al.* Reverse engineering of regulatory networks in human B cells. *Nat Genet* 2005; **37**:382-390.
21 Facchini LM, Penn LZ. The molecular role of Myc in growth and transformation: recent discoveries lead to new insights. *FASEB J* 1998; **12**:633-651.
22 Henriksson M, Luscher B. Proteins of the Myc network: essential regulators of cell growth and differentiation. *Adv Cancer Res* 1996; **68**:109-182.
23 Pascale RM, De Miglio MR, Muroni MR, *et al.* c-myc amplification in pre-malignant and malignant lesions induced in rat liver by the resistant hepatocyte model. *Int J Cancer* 1996; **68**:136-142.
24 De Miglio MR, Simile MM, Muroni MR, *et al.* Correlation of c-myc overexpression and amplification with progression of preneoplastic liver lesions to malignancy in the poorly susceptible Wistar rat strain. *Mol Carcinog* 1999; **25**:21-29.
25 Yaswen P, Goyette M, Shank PR, Fausto N. Expression of c-Ki-ras, c-Ha-ras, and c-myc in specific cell types during hepatocarcinogenesis. *Mol Cell Biol* 1985; **5**:780-786.
26 Wang Y, Wu MC, Sham JS, *et al.* Prognostic significance of c-myc and AIB1 amplification in hepatocellular carcinoma. A broad survey using high-throughput tissue microarray. *Cancer* 2002; **95**:2346-2352.
27 Abou-Elella A, Gramlich T, Fritsch C, Gansler T. c-myc amplification in hepatocellular carcinoma predicts unfavorable prognosis. *Mod Pathol* 1996; **9**:95-98.
28 Zhang XK, Huang DP, Qiu DK, Chiu JF. The expression of c-myc and c-N-ras in human cirrhotic livers, hepatocellular carcinomas and liver tissue surrounding the tumors. *Oncogene* 1990; **5**:909-914.
29 Gautier T, Fomproix N, Masson C, *et al*. Fate of specific nucleolar perichromosomal proteins during mitosis: cellular distribution and association with U3 snoRNA. *Biol Cell* 1994; **82**:81-93.
30 Azum-Gelade MC, Noaillac-Depeyre J, Caizergues-Ferrer M, Gas N. Cell cycle redistribution of U3 snRNA and fibrillarin. Presence in the cytoplasmic nucleolus remnant and in the prenucleolar bodies at telophase. *J Cell Sci* 1994; **107**(**Pt 2**):463-475.
31 Jimenez-Garcia LF, Segura-Valdez ML, Ochs RL, *et al*. Nucleologenesis: U3 snRNA-containing prenucleolar bodies move to sites of active pre-rRNA transcription after mitosis. *Mol Biol Cell* 1994; **5**:955-966.
32 Angelier N, Tramier M, Louvet E, *et al.* Tracking the interactions of rRNA processing proteins during nucleolar assembly in living cells. *Mol Biol Cell* 2005; **16**:2862-2871.
33 Savino TM, Gebrane-Younes J, De Mey J, Sibarita JB, Hernandez-Verdun D. Nucleolar assembly of the rRNA processing machinery in living cells. *J Cell Biol* 2001; **153**:1097-1110.
34 Calvisi DF, Conner EA, Ladu S, *et al.* Activation of the canonical Wnt/beta-catenin pathway confers growth advantages in c-Myc/E2F1 transgenic mouse model of liver cancer. *J Hepatol* 2005; **42**:842-849.
35 Dundr M, Olson MO. Partially processed pre-rRNA is preserved in association with processing components in nucleolus-derived foci during mitosis. *Mol Biol Cell* 1998; **9**:2407-2422.
36 Russell J, Zomerdijk JC. The RNA polymerase I transcription machinery. *Biochem Soc Symp* 2006 (73):203-216.
37 Tollervey D, Kiss T. Function and synthesis of small nucleolar RNAs. *Curr Opin Cell Biol* 1997; **9**:337-342.
38 Kasugai Y, Tagawa H, Kameoka Y, *et al.* Identification of CCND3 and BYSL as candidate targets for the 6p21 ampli-

fication in diffuse large B-cell lymphoma. *Clin Cancer Res* 2005; **11**:8265-8272.
39 Suzuki N, Zara J, Sato T, *et al.* A cytoplasmic protein, bystin, interacts with trophinin, tastin, and cytokeratin and may be involved in trophinin-mediated cell adhesion between trophoblast and endometrial epithelial cells. *Proc Natl Acad Sci USA* 1998; **95**:5027-5032.
40 Marcu KB, Bossone SA, Patel AJ. myc function and regulation. *Annu Rev Biochem* 1992; **61**:809-860.
41 Paria BC, Dey SK, Andrews GK. Antisense c-myc effects on preimplantation mouse embryo development. *Proc Natl Acad Sci USA* 1992; **89**:10051-10055.
42 Fomproix N, Gebrane-Younes J, Hernandez-Verdun D. Effects of anti-fibrillarin antibodies on building of functional nucleoli at the end of mitosis. *J Cell Sci* 1998; **111(Pt 3)**:359-372.
43 Hernandez-Verdun D. Nucleolus: from structure to dynamics. *Histochem Cell Biol* 2006; **125**:127-137.
44 Sirri V, Hernandez-Verdun D, Roussel P. Cyclin-dependent kinases govern formation and maintenance of the nucleolus. *J Cell Biol* 2002; **156**:969-981.
45 Sugihara K, Sugiyama D, Byrne J, *et al.* Trophoblast cell activation by trophinin ligation is implicated in human embryo implantation. *Proc Natl Acad Sci USA* 2007; **104**:3799-3804.
46 Fukuda MN, Nozawa S. Trophinin, tastin, and bystin: a complex mediating unique attachment between trophoblastic and endometrial epithelial cells at their respective apical cell membranes. *Semin Reprod Endocrinol* 1999; **17**:229-234.
47 Suzuki N, Nakayama J, Shih IM, *et al.* Expression of trophinin, tastin, and bystin by trophoblast and endometrial cells in human placenta. *Biol Reprod* 1999; **60**:621-627.
48 Hatakeyama S, Ohyama C, Minagawa S, *et al.* Functional correlation of trophinin expression with the malignancy of testicular germ cell tumor. *Cancer Res* 2004; **64**:4257-4262.
49 Yang S, Liu X, Yin Y, Fukuda MN, Zhou J. Tastin is required for bipolar spindle assembly and centrosome integrity during mitosis. *FASEB J* 2008; **22**:1960-1972.
50 Zhu DH, Wang JB. Cultivating of QSG-7701 cell line and comparing it with liver cancer cell. *Res Cancer Prev Treat* 1979; **5**:7-9.
51 Pan QW, Zhong SY, Liu BS, *et al.* Enhanced sensitivity of hepatocellular carcinoma cells to chemotherapy with a Smac-armed oncolytic adenovirus. *Acta Pharmacol Sin* 2007; **28**:1996-2004.
52 Guo SY, Shen X, Yang J, *et al.* TIMP-1 mediates the inhibitory effect of interleukin-6 on the proliferation of a hepatocarcinoma cell line in a STAT3-dependent manner. *Braz J Med Biol Res* 2007; **40**:621-631.
53 Alley MC, Scudiero DA, Monks A, *et al.* Feasibility of drug screening with panels of human tumor cell lines using a microculture tetrazolium assay. *Cancer Res* 1988; **48**:589-601.
54 Savino TM, Bastos R, Jansen E, Hernandez-Verdun D. The nucleolar antigen Nop52, the human homologue of the yeast ribosomal RNA processing RRP1, is recruited at late stages of nucleologenesis. *J Cell Sci* 1999; **112(Pt 12)**:1889-1900.

(**Supplementary information** is linked to the online version of the paper on the *Cell Research* website.)